scientific reports

Check for updates

OPEN

Perpendicular magnetic anisotropy in a single Dy adatom ferrimagnet

Alexander B. Shick[1]✉, Frantisek Maca[1], Itzhak Halevy[2] & Dominik Legut[3]

The electronic structure and magnetism of individual Dy atoms adsorbed on ferromagnetic (Gr)/Ni(111) substrate are investigated using a combination of the density functional theory with the Hubbard-I approximation to the Anderson impurity model (DFT+U(HIA)). The divalent Dy^{2+} adatom in f^{10} configuration with [$J = 8, L = 6, S = 2$] is found. The values of spin M_S=3.4 μ_B, orbital M_L=5.2 μ_B, and total M_J=8.6 μ_B magnetic moments calculated for the Dy *f*-shell are noticeably different from the atomic second Hund's rule. There is almost zero moment on (Gr)-atoms. The ferromagnetic Ni substrate moments are anti-aligned to the Dy 4*f*-shell moment. The X-ray absorption (XAS) and magnetic circular dichroism (XMCD) spectra are calculated and can be compared to the experimental data. The magnetic anisotropy energy (MAE) is calculated from the ground state energy difference for different directions of the magnetization, E[100] - E[001] = 3.5 meV and E[010] - E[001] = 2.2 meV. This large and positive MAE can be important for ultra-high density magnetic recording. The magnetization of Dy@(Gr)/Ni(111) is tilted with respect to the (Gr)/Ni(111) substrate normal by 38^o due to a competition between negative first and third order magnetic anisotropies and strong and positive second order magnetic anisotropies. Our studies assist in resolving ambiguities of conventional DFT+U applied to Dy on graphene. They can provide a viable route for further investigation and prediction of the rare-earth based magnetic nanostructures.

The unique magnetic properties of RE ions adsorbed on surfaces or embedded into molecular complexes, in virtue of their large spin and orbital magnetic moments and a gigantic magnetic anisotropy energy (MAE), provide a viable pathway for creating atomic-scale magnetic memories[1]. These so-called single-atom magnets (SAM), terbium (Tb), dysprosium (Dy), holmium (Ho) adatoms deposited on an insulating MgO surface exhibit a large uniaxial MAE, which acts as a barrier against the spontaneous reversal of the magnetic moments and enhances their magnetic lifetimes[2]. The Dy atoms deposited on the graphene on the top of Ir substrate also display a SAM behaviour[3]. Experimental research into 4*f* adatoms on graphene[3,4] and MgO[5–7] has been carried out for over resent years. Nevertheless, it remains challenging to explain theoretically the influence of the substrate and adsorption geometry on the 4*f*-shell charge and magnetic configurations and the XAS/XMCD spectra[8] without prior knowledge of the experimental data.

It is now well established[9] that density functional theory (DFT) methodologies fall short of describing the basic spin and orbital magnetic properties of the rare-earth (RE), including the RE-transition metal (TM) magnets, correctly. We have recently extended DFT to treat the *f*-electron materials (RE and actinides), making use of the charge self-consistent implementation of the DFT++ methodology[10] and applied it to Dy adatom on insulating MgO substrate[11]. In our approach, DFT is combined with an exact diagonalization of a single-impurity many-body quantum impurity model (the so-called Anderson model)[12](AIM) to account for the full structure of the f-orbital atomic multiplets.

This work aims to explain the spin and orbital characteristics of currently existing magnetic materials and to predict the properties of new materials yet to be synthesized experimentally. For example, we consider the electronic structure and magnetism of individual Dy atoms adsorbed on ferromagnetic graphene (Gr)/Ni(111) substrate. Graphene on Ni(111) is of particular interest because it can be epitaxially grown[13] and as a building block of spintronic devices[14]. Moreover, Dy exhibits a large magnetic anisotropy and has been used for single-atom magnets with a large magnetic anisotropy[3,6].

Our calculations reveal a change of Dy valence from Dy^{3+}, typical of RE-TM bulk magnets, to Dy^{2+} at the GR/Ni(111) surface, obtained self-consistently within DFT+U(HIA) calculations. The Dy atom adopts an f^{10} many-body ground state, $|J = 8, J_z = -7\rangle$, representing a clear deviation from the conventional Hund's rule configuration. Moreover, we find that the first-order, second-order, and third-order magnetic anisotropy constants have different signs, leading to competing magnetic anisotropy contributions. This competition

[1]FZU-Institute of Physics, Czech Academy of Science, Na Slovance 2, 18221 Prague, Czech Republic. [2]Nuclear Engineering Unit, Ben Gurion University of the Negev, 84105 Beer-sheva, Israel. [3]IT4Innovations and Nanotechnology Centre, CEET, VSB - Technical University of Ostrava, 17. listopadu 2172/15, 70800 Ostrava, Czech Republic. ✉email: shick@fzu.cz

results in a pronounced tilt of the Dy magnetic moment away from the crystallographic high-symmetry axes, a prediction that can be experimentally verified via the angular dependence of element-specific XMCD spectra. Together, these findings provide new microscopic insight into the electronic configuration and magnetic anisotropy of surface supported RE adatoms.

Results and discussion

To discern the spin and orbital magnetism of the rare-earth Dy adatom on GR/Cu(111) we make use of the $3 \times 3 \times 1$ supercell model with 36 Ni-atoms (4 layers) for the substrate, and the graphene layer with eighteen C atoms on the top of the Ni(111) surface. The graphene overlayer is placed in the so-called "HCP" (or "1-3") position, where one of the C atoms sits on the top of the Ni surface, and another is over the second Ni subsurface layer. The experimental Ni lattice constant of 4.705 a.u. is used. The rare-earth Dy atom is placed in the hollow position atop the graphene/Ni(111) surface. The top view of the supercell is shown in Fig. 1A.

The structure relaxation is performed using the Vienna ab initio simulation package (VASP[15]), employing the DFT exchange-correlation functional of Perdew, Burke, and Ernzerhof (PBE[16]) in combination with the projector augmented-wave method (PAW[17]). Assuming that localized 4*f* electrons have a negligible effect on the geometry, we used a rare-earth Lu adatom as a substitute for Dy, treating the 14 closed 4*f*-shell electrons of Lu as valence states. The atomic positions were relaxed until the forces on the Lu adatom, the carbon atoms of graphene, and the topmost two monolayers (ML) of Ni were reduced below 0.001 eV/Å. The use of Lu instead of Dy is further justified by comparison with previous total energy minimization calculations for Dy on graphene/Cu(111)[20], where the optimal distance of 4.23 a.u. is reasonably close to the optimized distance of 4.15 a.u. obtained for Lu on graphene/Ni(111).

The relaxed structural data obtained from the VASP simulations was used as input for further DFT+U(HIA) electronic structure calculations that employ the relativistic version of the full-potential linearized augmented plane-wave method (FP-LAPW)[18,19]. Further details of DFT+U(HIA) calculations are described in the "Theoretical Method" section. This two-step approach combines the speed and efficiency of the highly optimized VASP package with the state-of-the-art accuracy of the FP-LAPW method.

The results of DFT+U(HIA) calculations are shown in Table 1. The optimal distance $d_0 = 4.145$ a.u. between the Dy atom and the graphene surface is slightly reduced compared with the previously reported Dy@GR/Cu(111) case[20]. The spin $\langle M_S \rangle$, orbital $\langle M_L \rangle$, and the total ($\langle M_S \rangle$+$\langle M_L \rangle$) moments shown in Table 1 are noticeably different from what would be expected from the atomic second Hund rule. The *f*-shell moments are aligned with the 6*s* (0.05 μ_B) and 5*d* (0.09 μ_B) spin magnetic moments in the Dy "muffin-tin" . The spin polarisation of the C-atoms of graphene is very small, less than 0.04 μ_B, and directed along the Dy atom 6*s*5*d* polarisation. Remaining Ni and interstitial spin moments are anti-aligned to the 4*f* moment of Dy. The total non-*f* spin of -18.03 μ_B and orbital -1.80 μ_B are mainly the 3*d*-moments of the Ni substrate.

The spin-resolved *f*-projected (*f*DOS) DOS are shown in Fig. 1 (B) together with the *d*-projected (*d*DOS) of Dy and indicate the semi-atomic character of the *f*-states of Dy acquiring some *d*-occupation. Also, the partial DOS for the graphene C-atoms is shown in Fig. 1 (B). It indicates a significant n-doping due to the charge transfer to graphene and the metallic character of Dy@GR/Ni(111) similar to Dy@GR/Cu(111) case[20].

The Dy^{2+} valence state is not assumed a priori but instead emerges naturally from the self-consistent DFT+U(HIA) calculations. It corresponds to the many-body ground-state (GS) solution of Eq. (4). The GS is characterized by $N_f = 10$ (number of localized *f* electrons), quantum numbers $J = 8$, $L = 6$, $S = 2$ (total, orbital, and spin moments, respectively), and a Lande factor of $g_J = 1.25$. These values correspond to the f^{10} ionic configuration and define the Dy adatom valence as Dy^{2+}. The fact that Dy^{2+} is obtained self-consistently, rather than imposed as an input, underscores the reliability of the method in capturing the electronic configuration.

The *f*-electron occupation $n_f = 9.94$ calculated with the aid of Eq. (5) is consistent with the f^{10} configuration obtained from Eq. (4). The many-body GS of Eq. (4) is $|J = 8.0, J_z = -7.0\rangle$ with the total magnetic moment M_z= 8.72 μ_B. This value is consistent with the total $\langle M_S \rangle$ + $\langle M_L \rangle$ magnetic moment (cf. Table 1) calculated with the aid of Eq. (5).

Recently, the magnetic properties of Dy on a free-standing graphene were investigated with the aid of DFT+U[21]. Two different self-consistent solutions were found, the state with $n_f \approx 9.9$, $\langle M_S \rangle \approx 4\ \mu_B$, $\langle M_L \rangle \approx 5.9 \mu_B$, and another one with partially quenched $\langle M_L \rangle = 4.9 \mu_B$. They were interpreted to correspond $|J = 8, J_z = -8\rangle$ and $|J = 7, J_z = -7.0\rangle$ *f*-electron configurations. From the total energy difference between these two magnetic solutions, the $J = 7$ solution was found as the lowest energy state. The present DFT+U(HIA) calculations assist in resolving this ambiguity and allow us to identify this state as $|J = 8, J_z = -7\rangle$.

The self-consistently determined crystal field potential matrix Δ_{CF} can be expressed in terms of Wybourne's spherical tensor operators [22], and a set of Stevens crystal field parameters (CF) $[A_k^q \langle r^k \rangle]$ can be extracted[23]. The non-zero CF parameters $[A_k^q \langle r^k \rangle]$, and the exchange field Δ_{EX} are shown in Table 1. We used Eq. (4), with these parameters as an input for the Quanty code[24,25] to evaluate the $M_{4,5}$-edge XAS and XMCD spectra. The computed spectra are shown in Fig. 1C. They can be used to make a comparison of our predictions with the experimental data.

The magnetic anisotropy of Dy@Gr/Ni(111) is evaluated making use of the "two sublattices" model of 3*d*-4*f* intermetallics[26,27]. In this model, which is commonly used for the bulk rare-earth-transition metal ferrimagnets[27], the hamiltonian is divided in two parts. First, there is the 4*f* local Hamiltonian for the Dy,

$$\hat{H}_{4f} = \sum_{kq} A_k^q \langle r^k \rangle \Theta_k(J) \hat{O}_k^q + [2(g_J - 1)\mathrm{B}_{ex} + g_J \mathrm{B}_{ext}]\hat{J}\ , \tag{1}$$

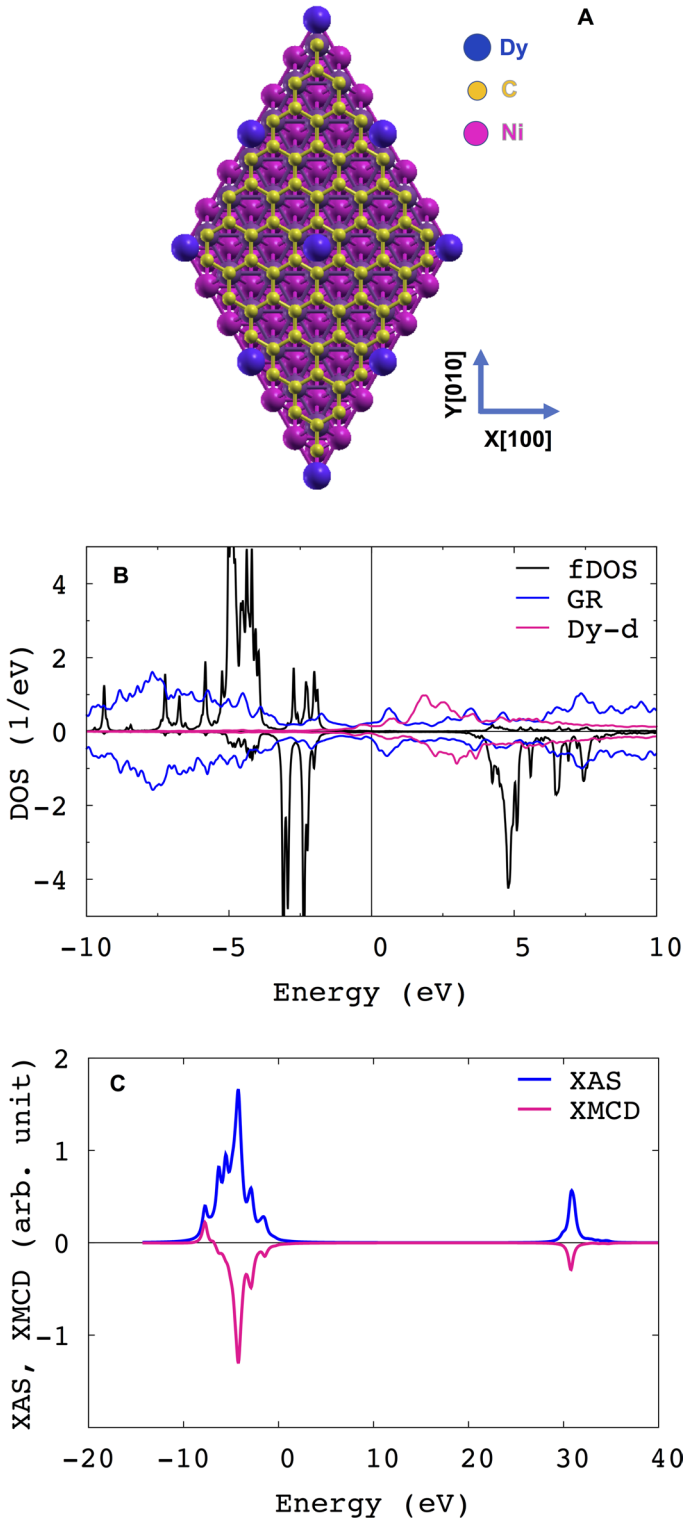

Fig. 1. Supercell model for rare-earth impurity on graphene/Ni(111) (Dy@GR/Ni). Dy atoms are shown in blue, C atoms are in gold, and Ni atoms in magenta (**A**); The spin-resolved *f*-projected (*f*DOS) DOS , The graphene and Dy-5*d* projected DOS (**B**); The $M_{4,5}$ edge XAS and XMCD spectra (normal incidence) (**C**) for Dy@GR/Ni.

where $\hat{O}_k^q$ are the Stevens operator equivalents, $\Theta_k(J)$ are the Stevens factors for a given ground state multiplet J, the exchange B_{ex} and the external B_{ext} magnetic fields are acting on the 4*f* shell. The magnitude of B_{ex} is equal to $\Delta_{\mathrm{EX}}/2$ in Eq. (4).

The second part, the 3*d* (Gr)/Ni(111) sublattice, is described by

Dy@GR/Ni	d_0	n_f	$\langle M_S \rangle$	$\langle M_L \rangle$	$\langle M_S \rangle$+$\langle M_L \rangle$
Dy	4.145	9.94	3.38	5.26	8.64
GR/Ni	4.136		-18.03	-1.80	-19.83
CEF	$A_2^0\langle r^2 \rangle$	$A_4^0\langle r^4 \rangle$	$A_6^0\langle r^6 \rangle$	$A_6^6\langle r^6 \rangle$	$\Delta_{\rm EX}$
(meV)	14.20	-4.19	-0.36	-8.50	11.0
MAE	K_1	K_2	K_3	K_4	$E_{MA}[010]$-$E_{MA}[001]$
(meV)	-8.39	11.80	-0.60	0.66	2.15
					$E_{MA}[100]$-$E_{MA}[010]$
					1.32

Table 1. Average distance d_0 (in a.u.) from the graphene overlayer on Ni(111) (GR/Ni), and between the graphene overlayer and the Ni surface, *f*-electron occupation n_f, spin $\langle M_S \rangle$, orbital $\langle M_L \rangle$, and the total $\langle M_S \rangle$ + $\langle M_L \rangle$ moments (in μ_B) for the Dy-atom. The non-f spin and the orbital magnetic moments, together with the total non-f magnetic moment **m** in the Dy@GR/Ni unit cell. The non-zero CF parameters $[A_k^q\langle r^k \rangle]$, and the exchange field $\Delta_{\rm EX}$ for Dy adatom on GR/Ni(111) (in meV). The magnetic anisotropy constants *K*, and the corresponding magnetic anisotropy energy (MAE, meV) for the Dy adatom on GR/Ni(111) (in meV).

$$\hat{H}_{3d} = -\mathbf{M_{3d}}\mathrm{B}_{ext} + K_{3d}(\theta_{3d}, \phi_{3d}) \ , \tag{2}$$

where M_{3d} and K_{3d} are the magnetization and the magnetic anisotropy of the Gr/Ni(111) substrate. The polar angles (θ_{3d}, ϕ_{3d}) define the direction of the magnetization $\mathbf{M}_{3d}$.

The Dy adatom contribution to the magnetic anisotropy $E_{MA}^{4f}(\theta, \phi) = \langle \hat{H}_{4f} \rangle$,

$$E_{MA}^{4f} = K_1 \sin^2\theta + K_2 \sin^4\theta + K_3 \sin^6\theta + K_4 \sin^6\theta \cos(6\phi) \ , \tag{3}$$

Note, that the direction of $\mathbf{M}_{3d}$ is anti-parallel to B_{ex} with $\theta_{3d} = \pi + \theta$ and $\phi_{3d} = \pi + \phi$ are expressed using the polar coordinates (θ, ϕ) which define the direction of B_{ex}.

The θ angular dependence of E_{MA}^{4f} with $\phi = \pi/2$ is shown in Fig. 2A. The ϕ angular dependence of E_{MA}^{4f} with $\theta = \pi/2$ is shown in Fig. 2B reflecting the in-plane sixfold C_{6v} symmetry. Fitting E_{MA}^{4f} angular dependence by Eq.(3), we obtain K_1 = -8.39 meV, K_2 = 11.80 meV, K_3 = -0.60 meV and K_4 = 0.66 meV. The K_1 and K_3 constants are negative, and the magnetic anisotropy E_{MA}^{4f} is dominated by the $K_2 \sin^4\theta$ term. The positive sign of K_4 leads to a nonzero basal angles $\phi = 30^o, 90^o$ for the minimal energy. The uniaxial MAE $= E_{MA}[010] - E_{MA}[001]$ = 2.2 meV and $= E_{MA}[100] - E_{MA}[001]$ = 3.5 meV are evaluated. The positive MAE sign indicates the perpendicular magnetic anisotropy for Dy@Gr/Ni(111).

As follows from the (θ, ϕ) angular dependence shown in Fig. 2, the magnetic anisotropy energy Eq.(3) for the Dy adatom on (Gr)/Ni(111) has minima at $\theta = 38^o, \phi = 30^o \pm 60^o$. The tilting angle θ is determined[28] by

$$\sin^2(\theta) = \frac{\sqrt{{K_2}^2 - 3K_1K_3'} - K_2}{3K_3'} \ ,$$

where $K_3' = K_3 - K_4$.

To evaluate the magnetic anisotropy K_{3d} of the (Gr)/Ni(111) substrate, we calculated the MAE for a GR/Ni_9/GR slab model (see Supplemental Material[29-36]). The slab MAE was found to be $\approx$ 0.18 meV, which is further reduced to $\approx$ 0.11 meV after appying the shape anisotropy correction. Thus, the magnetic anisotropy K_{3d} of the (Gr)/Ni(111) substrate is small and positive, and will be neglected in the following discussion. Furthermore, since M_{3d} is dominated by the spin contribution $\langle M_S \rangle$ (see Table 1), we also neglect the small anisotropy of the orbital moments $\langle M_L \rangle$ of the Ni substrate atoms.

The magnetic structure of the whole system is determined by the minimum of the total energy, a sum of Eq.(2) and Eq.(3). Since $K_{3d} \approx 0$, and in a zero external field, it is determined by the minima of the magnetic anisotropy energy Eq.(3) at $\theta = 38^o, \phi = 30^o \pm 60^o$. For the tilting angle $\theta = 38^o$ and $\phi = 90^o$, the 4*f*-magnetic moment $\mathbf{M}_{4f}$ is aligned at $\theta_{4f} = 36^o$ and $\phi_{4f} = 90^o$. Corresponding $\mathbf{M}_{3d}$ is aligned in the $Y - Z$ plane with $\theta_{3d} = 218^o$ and $\phi_{3d} = 270^o$. Thus, the Dy *f*-magnetic moment $\mathbf{M}_{4f}$ is essentially anti-parallel to the $\mathbf{M}_{3d}$. The total magnetization ($\mathbf{M}_{4f}$ plus $\mathbf{M}_{3d}$) of Dy@(Gr)/Ni(111) is tilted in the $Y - Z$ plane (Fig. 1A) to the surface normal direction by $\theta \approx 38^o$ and Dy and Ni moments remain almost anti-aligned. This prediction of magnetization tilt can be experimentally verified by measuring the angular dependence of element-specific XMCD signal intensities.

It should be noted that the present calculations are carried out at $T = 0$ K. Nevertheless, the uniaxial MAE of 2.15 meV can be used to qualitatively estimate the thermal stability of Dy@GR/Ni(111) at low temperatures within the framework of the Arrhenius-Neel law for thermally activated switching, $\tau = \tau_0 \exp(U_{rev}/k_BT)$ where τ is the magnetic lifetime, τ_0 is the characteristic attempt time between successive reversal events, and U_{rev} is the energy barrier for thermally assisted magnetization reversal. Using $U_{rev} = 2.15$ meV (the MAE) and $\tau_0 = 4.5 \times 10^{-9}$ s, taken from experimental data on Dy@GR/Ir(111)[2], we obtain for $T = 4$ K an estimated lifetime of $\tau \approx 3 \times 10^{-6}$ s.

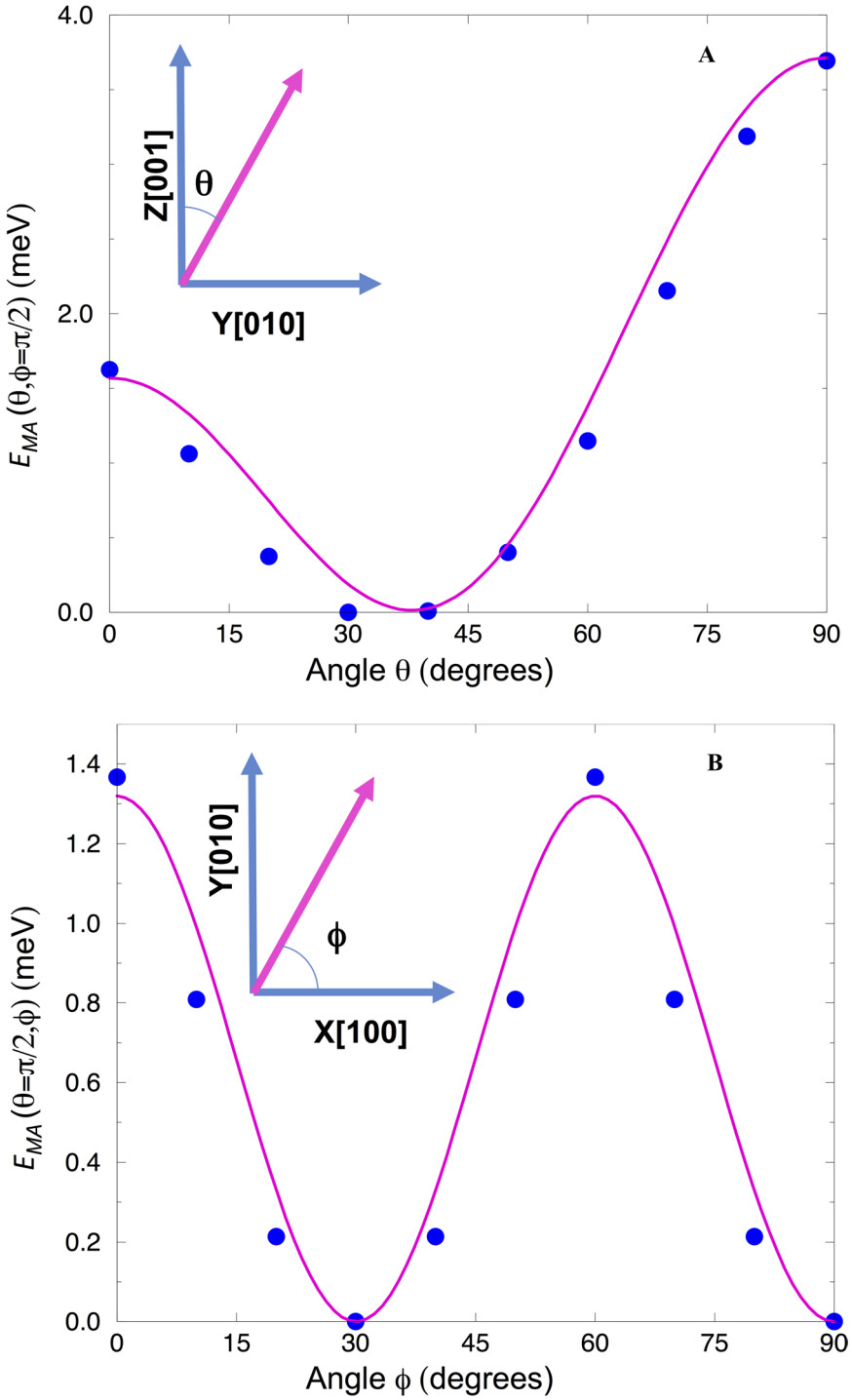

Fig. 2. $E^{4f}_{MA}(\theta, \phi = \pi/2)$ (A) and $E^{4f}_{MA}(\theta = \pi/2, \phi)$ for Dy adatom on graphene/Ni(111) (Dy@GR/Ni).

Summary

In summary, we address the electronic and magnetic structure and the magnetic anisotropy of Dy@Gr/Ni(111), making use of the DFT+U(HIA) methodology and a supercell model. The divalent Dy^{2+} adatom in f^{10} configuration with $[J = 8, L = 6, S = 2]$ and the Lande factor g_J=1.25 is found with $|J = 8.0, J_z = -7.0\rangle$ many-body ground state of Eq. (4). The values of spin M_S=3.4 μ_B, orbital M_L=5.2 μ_B, and total M_J=8.6 μ_B calculated for the Dy *f*-shell are noticeably different from the atomic second Hund's rule. There is almost zero moment on (Gr)-atoms. The ferromagnetic Ni substrate moments are anti-aligned to the Dy 4*f*-shell moment. The magnetic anisotropy energy (MAE) is calculated from the energy difference for different directions of the magnetization $E[010] - E[001]$ = 2.2 meV and $E[100] - E[001]$ = 3.5 meV. The magnetization of Dy@(Gr)/Ni(111) is tilted to the (Gr)/Ni(111) substrate normal by 38^o due to a competition between negative first and

third order magnetic anisotropies and strong and positive second order magnetic anisotropies. Our studies can provide a viable route for further investigation and prediction of the rare-earth single-atom magnets. The large and positive MAE in Dy@(Gr)/Ni(111) can be utilized for ultra-high-density magnetic recording.

Theoretical method

We employ recently proposed DFT+U(HIA) extension[11,20] of the DFT+U method in a rotationally invariant, full potential implementation[37,38]. In the DFT+U(HIA) approach, DFT is combined with the exact diagonalization of the Anderson impurity model[39]. Assuming the weakness of the hybridization between the localized 4*f*-electrons and the itinerant *s*, *p*, and *d*-states, the Anderson impurity model is reduced to the atomic limit and corresponds to the Hubbard-I approximation (HIA). The corresponding Anderson impurity model Hamiltonian can be written as,

$$\begin{aligned}\hat{H}_{\mathrm{imp}} &= \sum_{m\sigma} \epsilon_f f^{\dagger}_{m\sigma} f_{m\sigma} \\ &+ \sum_{mm\sigma\sigma'} \left[\xi \mathrm{l}\cdot\mathrm{s} + \hat{\Delta}_{\mathrm{CF}} + \frac{\Delta_{\mathrm{EX}}}{2}\hat{\sigma}_z\right]^{\sigma\ \sigma'}_{mm} f^{\dagger}_{m\sigma} f_{m'\sigma'} \\ &+ \frac{1}{2} \sum_{\substack{mmm''\\ m'''\sigma\sigma'}} U_{mmm''m'''} f^{\dagger}_{m\sigma} f^{\dagger}_{m'\sigma'} f_{m'''\sigma'} f_{m''\sigma},\end{aligned} \tag{4}$$

where $f^{\dagger}_{m\sigma}$ creates a 4*f* electron. The parameter ϵ_f ($= -\mu$, the chemical potential) defines the number of *f*-electrons. The ξ parameter specifies the 4*f*-SOC strength, and is taken from DFT calculations. Δ_{CF} is the crystal-field potential. These parameters are determined in the charge self-consistent DFT+U(HIA) calculations as described in Ref. [20,39]. Δ_{EX} is the strength of the exchange field acting on the 4*f* shell of Dy (see Supplemental material[29-36]). The last term in Eq.(4) describes the Coulomb interaction in the 4*f*-shell. The Slater integrals $F_0 = 7.00$ eV, and $F_2 = 9.77$ eV, $F_4 = 6.53$ eV, and $F_6 =$4.83 eV were chosen to parametrize the Coulomb interaction term. They correspond to the values for Coulomb $U = 7.00$ eV and exchange $J = 0.82$ eV.

The band Lanczos method[40] is employed to find the lowest-lying eigenstates of the many-body Hamiltonian H_{imp} and to calculate the one-particle Green's function $[G_{\mathrm{imp}}(z)]^{\sigma\ \sigma'}_{mm}$ in the subspace of the *f* orbitals at low temperature ($k_{\mathrm{B}}T = 1/500$ eV). The selfenergy $[\Sigma(z)]^{\sigma\ \sigma'}_{mm}$ is obtained from the inverse of the Green's function matrix $[G_{\mathrm{imp}}]$, and used to calculate the local Green's function $G(z)$ for the *f*-electrons,

$$[G(z)]_{\gamma_1\gamma_2} = \frac{1}{V_{\mathrm{BZ}}} \int_{\mathrm{BZ}} \mathrm{d}^3k \left[z + \mu - H_{\mathrm{DFT}}(\mathrm{k}) - \Sigma(z)\right]^{-1}_{\gamma_1\gamma_2}, \tag{5}$$

in a single-site approximation. With the aid of the local Greens function $G(z)$, we evaluate the occupation matrix $n_{\gamma_1\gamma_2} = -\frac{1}{\pi}\,\mathrm{Im}\int_{-\infty}^{E_{\mathrm{F}}} \mathrm{d}z\,[G(z)]_{\gamma_1\gamma_2}$. The matrix $n_{\gamma_1\gamma_2}$ is used to construct an effective DFT+*U* potential V_U, which is used in the Kohn–Sham equations

$$[-\nabla^2 + V_{\mathrm{DFT}}(\mathrm{r}) + V_U + \xi(\mathrm{l}\cdot\mathrm{s})]\Phi^b_{\mathrm{k}}(\mathrm{r}) = \epsilon^b_{\mathrm{k}}\Phi^b_{\mathrm{k}}(\mathrm{r}). \tag{6}$$

These equations are iteratively solved until self-consistency over the charge density is reached. In each iteration, a new value of the 4*f*-shell occupation is obtained from the solution of Eq. (6). Subsequently, a new self-energy $\Sigma(z)$ corresponding to the updated 4*f*-shell occupation is constructed. Finally, the next iteration is started by evaluating the new local Green's function, Eq. (5). Further details of our implementation and calculations can be found in the Supplemental material[29-36].

Data availability

The data used during the current study are available from the corresponding author on reasonable request.

Received: 26 May 2025; Accepted: 15 September 2025
Published online: 17 October 2025

References

1. Donati, F. & Heirich, A. J. A perspective on surface-adsorbed single atom magnets as atomic-scale magnetic memory. *Appl. Phys. Lett.* **119**, 160503 (2021).
2. Baltic, R. et al. Magnetic properties of single rare-earth atoms on graphene/Ir(111). *Phys. Rev. B* **98**, 024412 (2018).
3. Baltic, R. et al. Superlattice of Single Atom Magnets on Graphene. *Nano Lett.* **16**, 7610 (2016).
4. Piveta, M. et al. Measuring the Intra-Atomic Exchange Energy in Rare-Earth Adatoms. *Phys. Rev. X* **10**, 031054 (2020).
5. Donati, F. et al. Magnetic remanence in single atoms. *Science* **352**, 318 (2016).
6. Singha, A. et al. Engineering atomic-scale magnetic fields by dysprosium single atom magnets. *Nat. Commun.* **12**, 4179 (2021).
7. Donati, F. et al. Correlation between Electronic Configuration and Magnetic Stability in Dysprosium Single Atom Magnets. *Nano Lett.* **21**, 8266 (2021).
8. Uldry, A., Vernay, F. & Delley, B. Systematic computation of crystal-field multiplets for x-ray core spectroscopies. *Phys. Rev. B* **85**, 125133 (2012).
9. Locht, I. L. M. et al. *Phys. Rev. B* **94**, 085137 (2016).

10. Lichtenstein, A. I. & Katsnelson, M. I. Ab initio calculations of quasiparticle band structure in correlated systems: LDA++ approach. *Phys. Rev. B* **57**, 6884 (1998).
11. Shick, A. B., Belsch, E. & Lichtenstein, A. I. Magnetism and electronic structure of a Dy atom on a MgO(001) substrate. *Phys. Rev. B* **108**, L180408 (2020).
12. Hewson, A. The Kondo Problem to Heavy Fermions, Cambridge University Press, (1993).
13. Huttmann, F. et al. Magnetism in a graphene-4f - 3d hybrid system. *Phys. Rev. B* **95**, 075427 (2017).
14. Wu, Q. et al. Efficient Spin Injection into Graphene through a Tunnel Barrier: Overcoming the Spin-Conductance Mismatch. *Phys. Rev. Appl.* **2**, 044008 (2014).
15. Kresse, G. & Furthmuller, J. Efficient iterative schemes for ab initio total-energy calculations using a plane-wave basis set. *Phys. Rev. B* **54**, 11169 (1996).
16. Perdew, J. P., Burke, K. & Ernzerhof, M. Generalized Gradient Approximation Made Simple. *Phys. Rev. Lett.* **77**, 3865 (1996).
17. Blochl, P. E. Projector augmented-wave method. *Phys. Rev. B* **50**, 17953 (1994).
18. Wimmer, E., Krakauer, H., Weinert, M. & Freeman, A. J. Full-potential self-consistent linearized-augmented-plane-wave method for calculating the electronic structure of molecules and surfaces: O_2 molecule. *Phys. Rev. B.* **24**, 864 (1981).
19. Shick, A. B., Novikov, D. L. & Freeman, A. J. Relativistic spin-polarized theory of magnetoelastic coupling and magnetic anisotropy strain dependence: Application to Co/Cu(001). *Phys. Rev. B* **56**, R14259 (1997).
20. Shick, A. B., Kolorenc, J., Denisov, A. Y. & Shapiro, D. S. Magnetic anisotropy of a Dy atom on a graphene/Cu(111) surface. *Phys. Rev. B* **102**, 064402 (2020).
21. Carbone, J. P., Bouaziz, J., Bihlmayer, G. & Blugel, S. Magnetic properties of 4f adatoms on graphene: Density functional theory investigations. *Phys. Rev. B* **108**, 174431 (2023).
22. Wybourne, B. G. *Spectroscopic properties of Rare Earth* (Interscience publishers, New York, 1965).
23. Delange, P., Biermann, S., Miyake, T. & Pourovskyi, L. Crystal field splittings in rare earth-based hard magnets: an ab-initio approach. *Phys. Rev. B* **96**, 155132 (2017).
24. Haverkort, M. W., Zwierzcki, M. & Andersen, O. K. Multiplet ligand-field theory using Wannier orbitals. *Phys. Rev. B* **85**, 165113 (2012).
25. https://quanty.org
26. Herbst, J. F. $R_2Fe_{14}B$ materials: Intrinsic properties and technological aspects. *Rev. Mod. Phys.* **63**, 819 (1991).
27. Yoshioka, T. & Tsuchiura, H. Site-specific magnetic anisotropies in $R_2Fe_{14}B$ systems. *Appl. Phys. Lett.* **112**, 162405 (2018).
28. Kuzmin, M. D. & Tishin, A. M. in *Handbook of Magnetic Materials*, (ed. Buschow, K. H. J.) Vol. 17, 17003 (2008).
29. MacDonald, A., Pickett, W. & Koelling, D. A linearised relativistic augmented-plane-wave method utilising approximate pure spin basis functions. *J. Phys. C: Solid State Phys.* **13**, 2675 (1980).
30. Ishizuka, J., Sumita, S., Daido, A. & Yanese, Y. Insulator-metal transition and topological superconductivity in UTe_2 from a first-principles calculation. *Phys. Rev. Lett.* **123**, 217001 (2019).
31. Khomyakov, P. A. et al. First-principles study of the interaction and charge transfer between graphene and metals. *Phys. Rev. B* **79**, 195425 (2009).
32. Chikazumi, S. *Physics of Ferromagnetism* 655 (Clarendon Press, Oxford University Press, Oxford, 1997).
33. Liechtenstein, A. I., Katsnelson, M., Antropov, V. & Gubanov, V. Local spin density functional approach to the theory of exchange interactions in ferromagnetic metals and alloys. *J. Magn. Magn. Mater* **67**, 65 (1987).
34. Khmelevskyi, S., Shick, A. B. & Mohn, P. Element-specific analysis of the magnetic anisotropy in Mn-based antiferromagnetic alloys from first principles. *Phys. Rev. B* **83**, 224419 (2011).
35. Barla, A. et al. Complex magnetic exchange coupling between Co nanostructures and Ni(111) across epitaxial graphene. *ACS Nano* **10**, 1101 (2016).
36. Maca, F., Shick, A. B., Redinger, J., Podloucky, R. & Weinberger, P. The influence of hydrogen adsorption on magnetic properties of Ni/Cu(001) surface. *Chechoslovak J. of Phys.* **53**, 33 (2003).
37. Shick, A. B., Liechtenstein, A. I. & Pickett, W. E. Implementation of the LDA+U method using the full-potential linearized augmented plane-wave basis. *Phys. Rev. B* **60**, 10763 (1999).
38. Shick, A. B. & Pickett, W. E. Magnetism, Spin-Orbit Coupling, and Superconducting Pairing in UGe_2. *Phys. Rev. Lett.* **86**, 300 (2001).
39. Shick, A. B., Fujimori, S.-I. & Pickett, W. E. UTe_2: a nearly insulating half-filled j=5/2, $5f^3$ heavy fermion metal. *Phys. Rev. B* **103**, 125136 (2021).
40. Kolorenc, J., Poteryaev, A. I. & Lichtenstein, A. I. Valence-band satellite in ferromagnetic nickel: LDA+DMFT study with exact diagonalization. *Phys. Rev. B* **85**, 235136 (2012).

Acknowledgements

We acknowledge stimulating discussions with Dr. A. Barla. This work was co-funded by the European Union and the Czech Ministry of Education, Youth and Sports (Project TERAFIT - CZ.02.01.01/00/22_008/0004594). We acknowledge partial support provided by the Czech Science Foundation (GACR) Grant No. 24-11992S. DL acknowledges the project e-INFRA CZ (ID:90254) by the Czech Ministry of Education, Youth and Sports.

Author contributions

AS, IH, and DL conceived and supervised the project. AS, FM, and DL performed the computations. All authors contributed to the interpretation of the data and the writing of the manuscript.

Declarations

Competing interests

The authors declare no competing interests.

Additional information

Supplementary Information The online version contains supplementary material available at https://doi.org/10.1038/s41598-025-20466-z.

Correspondence and requests for materials should be addressed to A.B.S.